Computation of transverse injection into supersonic crossflow with various boundary layer thickness

Yekaterina Moisseyeva, Altynshash Naimanova, and Asel Beketaeva

***Abstract*—**Supersonic turbulent multispecies flow with transverse jet injection is numerically investigated. On the basis of the developed model the pattern of the vortex system formation is studied in detail. As a result, new vortices formed in the recirculation zone ahead of the jet are identified as well as their effect on the mixing layer. The effect of the boundary layer thickness on the vortex system is also studied, and the value of the boundary layer thickness, for which there is an additional multi-structural separation zone ahead of the jet, is determined. The formation of the lateral vortex pairs generated by the upstream vortices, convection of these vortex systems downstream and their effect on the mixing layer are revealed in dependence of the boundary layer thickness.

***Keywords*—**boundary layer, mixing layer, supersonic flow, turbulence.

I. Introduction

THE study of the transverse injection into a supersonic flow is an important issue in the modeling of the supersonic combustion in scramjets. Analysis of effect of regime parameters, for example such as injection pressure ratio, type of injected gas, location of injection and state of incoming boundary layer, on the jet/free stream interaction allows enhancing supersonic mixing efficiency. In spite of many studies, the effect of the boundary layer thickness on the mixing layer has not yet been clearly identified. It is well known from literature [1] that the interaction of the transverse jet with the incoming flow is unsteady due to jet shear layer instabilities coupled with incoming boundary layer. Within the scope of this paper steady features of jet interaction are investigated.

The general structure of the supersonic free stream with the transverse injected jet is shown in Fig. 1 [2,3]. The turbulent boundary layer ahead of the injector is characterized by the two counter-rotating vortices, primary upstream vortex (PUV) and secondary upstream vortex (SUV) [1-4]. These vortices are convected downstream by the free stream, forming the horseshoe vortices and wake vortices in the region behind the jet injector.

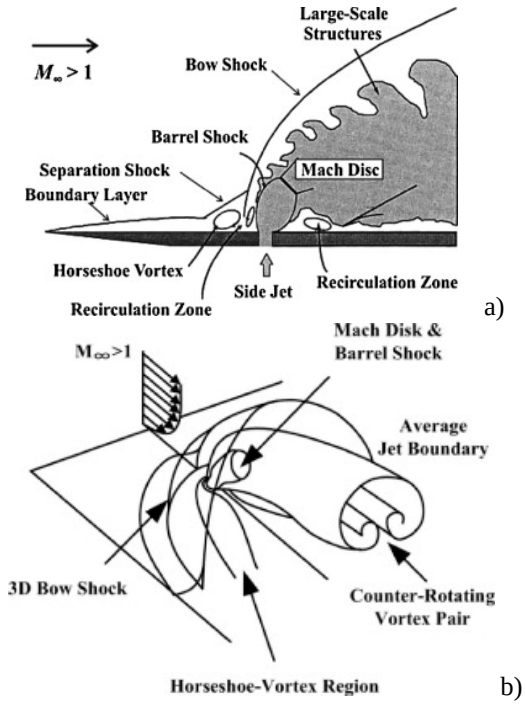

Fig. 1 schematic diagram of the flowfield: a) in the symmetry section xz [2], b) spatial structure [3]

However, there are some works [1,5-10] revealing the additional vortex structures in dependence of the regime and geometry parameters. The present investigation aims to study the effect of the incoming boundary layer thickness on the jet interaction phenomenon, particularly on the formation of the vortical systems behind the injector which are governed by the state of the incoming boundary layer and affect the mixing layer.

This work is supported in part by the Ministry of Education and Science of Republic of Kazakhstan under grant funding of fundamental research in the natural science field («Mathematical modeling and numerical solution of some problems of spatial sub- and supersonic turbulent flows with jets injection», 2015-2017, State Registration No. 0115PK00641).

Ye. Moisseyeva is with the Al-Farabi Kazakh National University, Almaty, Kazakhstan (corresponding author to provide phone: 8(727)272-00-48; e-mail: k.moisseyeva@gmail.com).

A. Naimanova is with the Institute of Mathematics and Mathematical Modeling MES RK, Almaty, Kazakhstan (e-mail: alt_naimanova@yahoo.com).

A. Beketaeva is with the Al-Farabi Kazakh National University, Almaty, Kazakhstan (e-mail: azimaras@mail.ru).

II. Physical Models and Numerical Methods

A. Governing Equations

Basic equations for the problem are the system of the three-dimensional Favre averaged Navier-Stokes equations for the compressible turbulent multispecies gas in the Cartesian coordinate system written in the conservative form as

$$\frac{\partial \vec{U}}{\partial t} + \frac{\partial\left(\vec{E} - \vec{E}_v\right)}{\partial x} + \frac{\partial\left(\vec{F} - \vec{F}_v\right)}{\partial y} + \frac{\partial\left(\vec{G} - \vec{G}_v\right)}{\partial z} = 0, \qquad (1)$$

where the vectors of the dependent variables and the vector fluxes are defined by

$$\vec{U} = \left(\rho, \rho u, \rho v, \rho w, E_t, \rho Y_k\right)^T,$$
$$\vec{E} = \left(\rho u, \rho u^2 + p, \rho uv, \rho uw, \left(E_t + p\right)u, \rho u Y_k\right)^T,$$
$$\vec{F} = \left(\rho v, \rho uv, \rho v^2 + p, \rho vw, \left(E_t + p\right)v, \rho v Y_k\right)^T,$$
$$\vec{G} = \left(\rho w, \rho uw, \rho vw, \rho w^2 + p, \left(E_t + p\right)w, \rho w Y_k\right)^T,$$
$$\vec{E}_v = \left(0, \tau_{xx}, \tau_{xy}, \tau_{xz}, u\tau_{xx} + v\tau_{xy} + w\tau_{xz} - q_x, J_{kx}\right)^T,$$
$$\vec{F}_v = \left(0, \tau_{xy}, \tau_{yy}, \tau_{yz}, u\tau_{xy} + v\tau_{yy} + w\tau_{yz} - q_y, J_{ky}\right)^T,$$
$$\vec{G}_v = \left(0, \tau_{xz}, \tau_{yz}, \tau_{zz}, u\tau_{xz} + v\tau_{yz} + w\tau_{zz} - q_z, J_{kz}\right)^T.$$

The components of the viscous stress tensor are given as

$$\tau_{xx} = \frac{2\mu}{3\mathrm{Re}}\left(2u_x - v_y - w_z\right),\ \tau_{yy} = \frac{2\mu}{3\mathrm{Re}}\left(2v_y - u_x - w_z\right),$$
$$\tau_{zz} = \frac{2\mu}{3\mathrm{Re}}\left(2w_z - u_x - v_y\right),\ \tau_{xy} = \tau_{yx} = \frac{\mu}{\mathrm{Re}}\left(u_y + v_x\right),$$
$$\tau_{xz} = \tau_{zx} = \frac{\mu}{\mathrm{Re}}\left(u_z + w_x\right),\ \tau_{yz} = \tau_{zy} = \frac{\mu}{\mathrm{Re}}\left(v_z + w_y\right).$$

The heat flux is defined by

$$q_x = \left(\frac{\mu}{\mathrm{PrRe}}\right)\frac{\partial T}{\partial x} + \frac{1}{\gamma_\infty M_\infty^2}\sum_{k=1}^{N} h_k J_{xk},$$
$$q_y = \left(\frac{\mu}{\mathrm{PrRe}}\right)\frac{\partial T}{\partial y} + \frac{1}{\gamma_\infty M_\infty^2}\sum_{k=1}^{N} h_k J_{yk},$$
$$q_z = \left(\frac{\mu}{\mathrm{PrRe}}\right)\frac{\partial T}{\partial z} + \frac{1}{\gamma_\infty M_\infty^2}\sum_{k=1}^{N} h_k J_{zk},$$

and the diffusion flux is determined by

$$J_{kx} = -\frac{\mu}{Sc\mathrm{Re}}\frac{\partial Y_k}{\partial x},\ J_{ky} = -\frac{\mu}{Sc\mathrm{Re}}\frac{\partial Y_k}{\partial y},$$
$$J_{kz} = -\frac{\mu}{Sc\mathrm{Re}}\frac{\partial Y_k}{\partial z}.$$

The pressure and the total energy are given as

$$p = \frac{\rho T}{\gamma_\infty M_\infty^2 W},\ E_t = \frac{\rho h}{\gamma_\infty M_\infty^2} - p + \frac{1}{2}\rho\left(u^2 + v^2 + w^2\right).$$

The specific enthalpy and the specific heat at constant pressure of the *k*th species are

$$h_k = h_k^0 + \int_{T_0}^{T} c_{pk}\,dT,\ c_{pk} = C_{pk}\left(\sum_{k=1}^{N}\frac{Y_k}{W_k}\right)$$

where the molar specific heat is written in the polynomial form as

$$C_{pk} = \sum_{i=1}^{5}\overline{a}_{jk}T^{(j-1)},$$

the coefficients $\overline{a}_{jk}$ are taken from the thermodynamic tables JANAF [11].

The viscosity coefficient is defined as a sum of the laminar and turbulent viscosity coefficients: $\mu = \mu_l + \mu_t$, where μ_l is determined by Wilke formula, and μ_t is determined by the $k-\omega$ turbulent model with compressibility effects in the turbulent parameters characterizing the local equilibrium.

In the system (1) ρ, u, v, w, T represent the density, components of the velocity vector, and the temperature, respectively. Y_k and W_k are the mass fraction and the molecular weight of the *k*th species, where index of *k*th species relates to H_2, O_2, N_2; namely, $k = 1$ stands for H_2, $k = 2$ stands for O_2, $k = 3$ stands for N_2. γ is the adiabatic parameter, *M* is the Mach number, Re is the Reynolds number, is the Prandtl number, and Sc is the Schmidt number. Index ∞ indicates parameters of the main flow.

The system (1) is written in a nondimensional form. Constitutive parameters are parameters of the main flow at the inlet (u_∞, ρ_∞, T_∞). The injector diameter *d* is chosen as the characteristic length.

B. Boundary Conditions

The initial conditions coincide with the boundary conditions at the flowfield entrance. At the flowfield entrance, the parameters of the free stream are given as

$$p = p_\infty,\ T = T_\infty,\ u = M_\infty\sqrt{\frac{\gamma_\infty R_0 T_\infty}{W_\infty}},\ v = 0,\ w = 0,$$
$$Y_k = Y_{k\infty},\ W_k = W_{k\infty},\ x = 0,\ 0 \le y \le H_y,\ 0 \le z \le H_z$$

Also the boundary layer is given near the wall. The longitudinal velocity component in the viscous sublayer [12] is determined by

$$u = 0.1\left(\frac{z}{\delta_2}\right) + 0.9\left(\frac{z}{\delta_2}\right)^2,$$
$$x = 0, 0 \le y \le H_y, 0 \le z \le \delta_2,$$

where $\delta_2 = 0.16\delta_1$ is the viscous sublayer thickness [13], $\delta_1 = 0.37x(\mathrm{Re}x)^{-0.2}$ is the boundary layer thickness [14].

In the turbulent boundary layer, the 1/7th power law is used

$$u = \left(\frac{z}{\delta_1}\right)^{1/7}, \; x = 0, \; 0 \le y \le H_y, \; \delta_2 < z \le \delta_1.$$

Depending on the velocity distribution [15], the temperature and density values are defined as

$$T = T_w + u(1 - T_w), \; \rho = \frac{1}{T},$$

where $T_w = 1 + r\frac{\gamma - 1}{2}M_\infty^2$ is the temperature at the wall, $r = 0.88$ is the temperature coefficient of restitution.

At the injector, the parameters of the jet are given as

$$p = np_\infty, \; T = T_0, \; u = 0, \; v = 0, \; w = M_0\sqrt{\frac{\gamma_0 R_0 T_0}{W_0}},$$
$$Y_k = Y_{k0}, \; W_k = W_{k0}, \; z = 0, \; \left|x^2 + y^2\right| \le R$$

where $n = p_0 / p_\infty$ refers to the pressure ratio.

The non-reflecting boundary conditions are adopted on the flow field exit [16]. The adiabatic no-slip boundary condition on the wall and the symmetry boundary condition on the symmetry faces are specified.

Here H_x, H_y and H_z refer to the length, width and height of the computational domain, respectively. R is the injector radius.

C. Numerical Schemes

Numerical solution of (1) is performed in two steps. The methodology can be found in [17-18]. At the first step the thermodynamic parameters (ρ, u, v, w, E_t) and at the second step the mass fractions Y_k are resolved. For the approximation of the convective terms, the ENO scheme of the third order is applied. The central differences of the second order of accuracy have been used for the approximation of the second derivatives. The obtaining system of equations is solved by the factorization using the matrix sweep method for the vector of the thermodynamic parameters and the tridiagonal inversion for the vector of the mass fractions. The temperature field is calculated from the known values of the variables $\vec{U}$, i.e. ρ, u, v, w, E_t, Y_k, with the use of the Newton-Raphson iterative method with the quadratic rate of convergence [19].

III. Results and Discussion

The flowfield without hydrogen jet is computed at first to validate the reliability of the mathematical model and numerical method with following free-stream parameters from the experiment by [20]: $\mathrm{Pr} = 0.9$, $\gamma = 1.4$, $\mathrm{Re} = 6.31 \cdot 10^4$, $M_\infty = 4$, $T_\infty = 500K$.

The obtained total pressure distribution and velocity profile in turbulent boundary layer is given in Fig. 2. Measurement is carried out near the wall in the symmetry section at the point where the boundary layer thickness is $\delta_1 = 2.7$ calibers ($z^+ = 5694$). Here $z^+ = zu_\tau \mathrm{Re}$ refers to dimensionless vertical distance (wall variable), $u_\tau = (0.5C_f)^{1/2}$ refers to friction velocity, $C_f = 0.0576(\mathrm{Re}\,x)^{-1/5}$ [14].

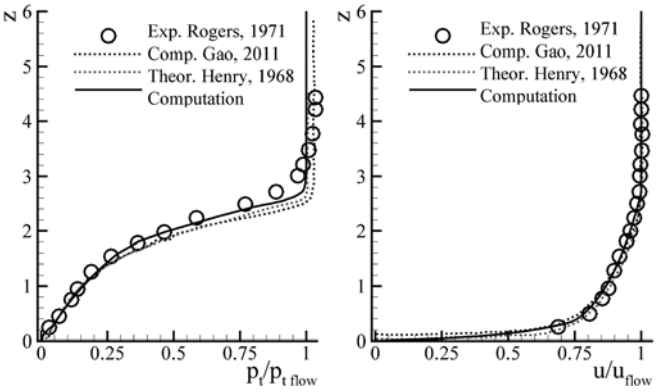

Fig. 2 boundary layer characteristics near wall in symmetry section, normal to y-axis, in channel without jet injection: results of [20-22] and numerical computation: a) total pressure distribution, b) velocity profile

It can be seen that the total pressure distribution (Fig. 2a) and velocity profile (Fig. 2b) agree well with the experimental data [20] and analytical and numerical calculations [21-22], that indicates the reliability of the numerical scheme and turbulence model.

Thereafter, the flowfield with hydrogen jet is simulated. According to [20], the center of the jet injection nozzle is placed at the point where the boundary layer thickness is $\delta_{1j} = 2.7$. The jet parameters is also specified according to the experiment [20]: $M_0 = 1$, $T_0 = 1300K$; ratio of jet dynamic pressure to free-stream dynamic pressure $q \equiv \rho_0 \vec{V}_0^2 / \rho_\infty \vec{V}_\infty^2 = 1.0$ which corresponds to $n = 15.61$; $d = 1.05mm$. The computational domain is described by following: $H_x = 20$, $H_y = 15$, $H_z = 10$ refer to the length, width and height of the domain; $x_0 = 10$, $y_0 = 7.5$ are the coordinates of the nozzle center.

Fig. 3 represents the streamlines and hydrogen mass fraction distribution in the symmetry section, normal to the y-axis. Most transverse jet-in-crossflow studies, for example [1-4], observed the presence of two vortices that are formed in the boundary layer separation. There is a few works [1,5-8] describing the tertiary vortex. However, Fig. 3a shows two upstream vortex pairs (V_1-V_4, V_2-V_3). The vortices V_2 and V_3 adjacent to the wall rotate counterclockwise and the vortices V_1 and V_4 rotate clockwise. The mechanism of their formation is the following. The first vortex V_1 is formed due to the boundary layer separation ahead of the jet. The interaction of the expanding jet with the λ-shock results in the formation of the second vortex V_2. Fig. 3a shows that these vortices are counter rotating. In the region of the λ-shock, the flow diverges in all directions, and its major part turns toward the wall and penetrates into the reverse separated flow region. After reaching the wall surface, the flow diverges in the opposite directions, forming the reattachment line R_1. For the recirculation flow moving from the reattachment line R_1 there is the second separation of the boundary layer with the formation of the vortex V_3. Furthermore, the flow deflects upward due to the vortex V_3, and also the main flow interacts from above with the vortex V_1. It results in the split of the V_1 into two vortices, which forms V_4.

The effect of the upstream vortex system on the jet and free stream mixing process is demonstrated by the distribution of the hydrogen mass fraction. Fig. 3b shows that the hydrogen is drifted upstream by the horseshoe vortices V_1-V_4 up to the separation line.

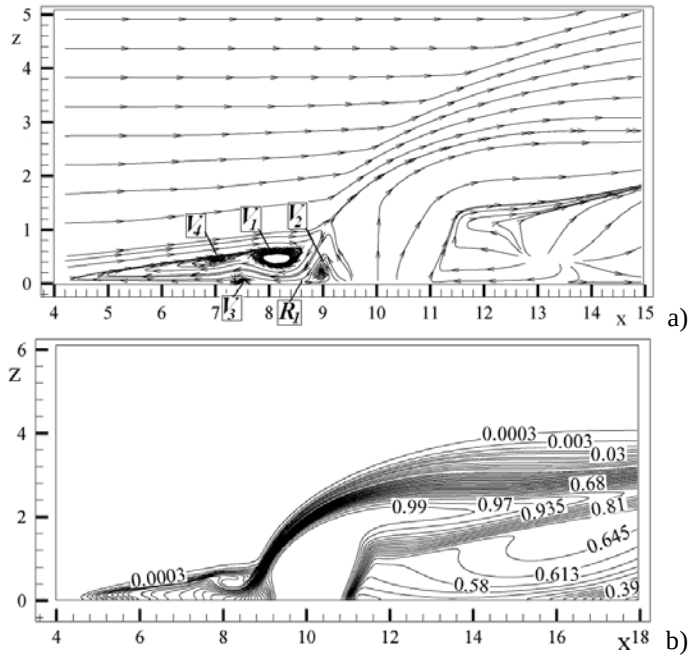

Fig. 3 streamlines (a) and mass fraction (b) in symmetry section, normal to y-axis, δ_{1j}=2.7

Fig. 4 represents the streamlines and hydrogen mass fraction distribution behind the jet in the section yz (x=13.835). The formation of the vortex V_5 is induced by the fact that a low-pressure region is formed near the wall directly behind the jet, and the free stream tends to pass into this region. The vortex V_1 is convected by the main flow and divided forming the system V_6. The emergence of vortices V_7 is due to the lateral flow of the vortex V_3. A minor size of these vortices is determined by the fact that the size of the vortex V_3 is also small. The vortex pair V_8 is generated by the vortex V_2. The numerical experiments reveal the offset of the vortices V_8 behind the barrel structure to the symmetry plane, while the vortices V_6 and V_7 move away from the symmetry plane as they are convected downstream.

The vortices V_8 (with the rotation centers in the mixing layer) increase in size downstream. The growth of the vortices near the jet is apparently provided by the significant gradients in pressure at the edge between the jet and free stream. From Fig. 4a it is also noticeable that the vortex systems V_6 and V_7 are a kind of cavity for vortex V_8 growth, i.e. the cavity increases as the vortices V_6 and V_7 moves away from the symmetry plane, and according to that the vortex V_8 enlarges.

The effect of the lateral vortex systems on the mixing layer is demonstrated in Fig. 4b. The core of the maximum values of the hydrogen mass fraction decreases downstream, while the mixing region expands. The comparison of Fig. 4a with Fig. 4b shows that the hydrogen is mainly accumulated in the area of the vortices V_8. Also, Fig. 4b demonstrates the effect of the vortices V_6 and V_7 forming the cavity on the mixing layer. The numerical calculations show that the drift of the hydrogen to the lateral sides is mainly made by the vortices V_6 and V_7.

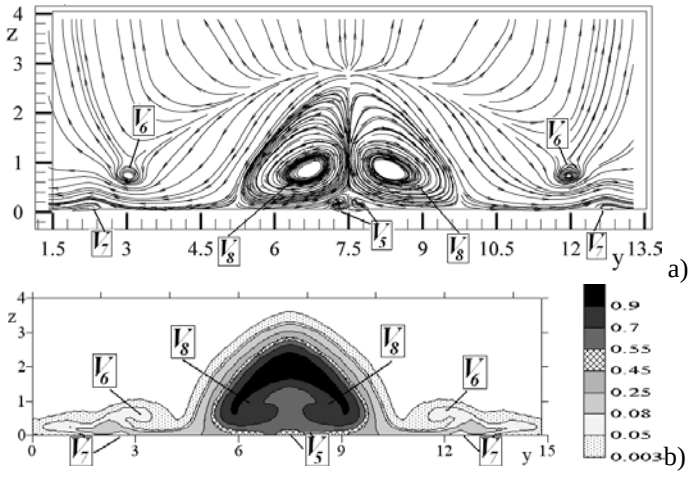

Fig. 4 streamlines (a) and mass fraction (b) in section x=13.835, normal to x-axis, δ_{1j} =2.7

It should be noted that in [9] there are the additional vortices at the top and bottom of the mixing region behind the jet for a monatomic gas for the pressure ratio n=10 and higher. However, the above analysis reveals that in the present study the additional vortex systems in these regions are not observed. Apparently, the absence of these vortices is explained by the fact that the computations are performed with

the thick boundary layer (δ_1=2.6 at the entrance), since in [9] the boundary layer thickness at the entrance was δ_1=1, Re=$1.87\cdot10^7$.

The numerical experiments performed at smaller thickness of the boundary layer show a decrease in the number of the upstream vortices. For example, the center of the jet injection nozzle is placed at the point where the value of the boundary layer thickness in the channel without jet injection was δ_{1j}=0.616, Figs. 5, 6. In this case, the results for the thin boundary layer reveal the two vortices V_1 and V_2 and deflected streamlines near the wall (Fig. 5a). Obviously, the flow deflection is not sufficient to divide the vortex V_1. Behind the jet, Fig. 5a demonstrates the formation of the vortex V_9 at the bottom of the mixing region, which is also obtained in [9]. This vortex is formed due to the interaction of the jet with the ascending flow under the jet. In the cross section (Fig. 6a) the vortex systems are qualitatively similar to described above for δ_{1j}=2.7 (Fig. 4a).

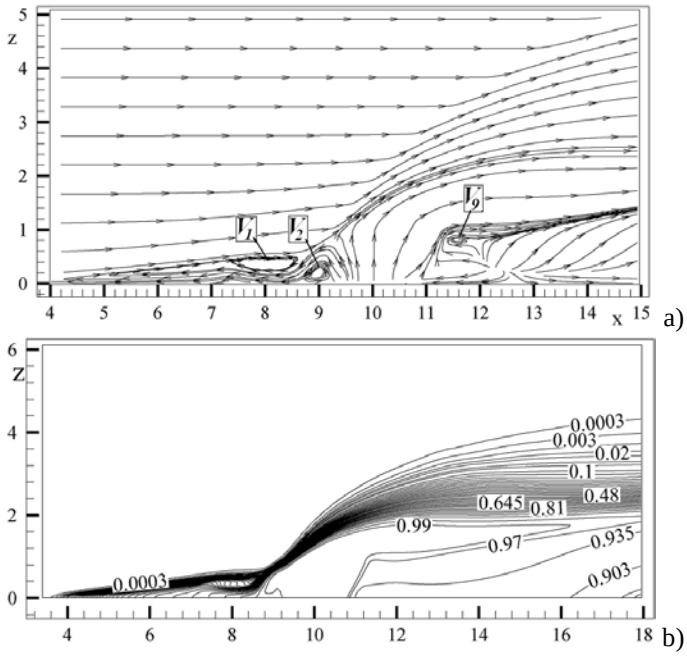

Fig. 5 streamlines (a) and mass fraction (b) in symmetry section, normal to y-axis, δ_{1j}=0.616

Comparison of Fig. 3b and Fig. 5b demonstrates that the distribution of the hydrogen mass fraction by the horseshoe vortices is further upstream than that for the thick boundary layer. Behind the jet injection, for δ_{1j}=2.7 in the region near the wall both hydrogen and airflow are observed, while for δ_{1j}=0.616 there is only hydrogen. So, the values of the hydrogen mass fraction near the wall are significantly higher than in the case of the thick boundary layer (Y_1=0.903 for δ_{1j}=0.616, Y_1=0.39 for δ_{1j}=2.7). Thus, for the thin boundary layer the mixing occurs mainly at the top of the mixing layer, and the major part of hydrogen is located near the wall. Also, comparison of Fig. 3b and Fig. 5b shows that the jet penetrates slightly higher for δ_{1j}=0.616. In the cross section (x=13.385, Figs. 4b, 6b), the mixing region for δ_{1j}=2.7 is larger than that for δ_{1j}=0.616. The maximum hydrogen concentrations for δ_{1j}=2.7 are accumulated in the jet core, while for δ_{1j}=0.616 the hydrogen mass fraction Y=0.55 achieves the lateral boundaries.

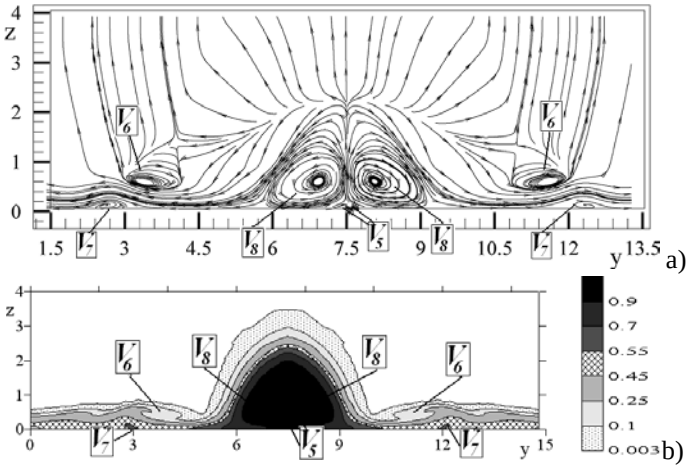

Fig. 6 streamlines (a) and mass fraction (b) in section x=13.835, normal to x-axis, δ_{1j} =0.616

IV. Conclusion

Thus, the computational experiments on identification of the mechanism of formation of vortex system show a significant effect of the boundary layer thickness on vortex structures and mixing layer. However, there is strong need to examine wall pressure in comparison with experimental data to confirm the separation zone length and the presence of the additional vortex structures. Further studies will aim to identify the correctness of the separated region flow filed.

References

[1] E. Erdema and K. Kontis, "Numerical and experimental investigation of transverse injection flows", *Shock Waves*, vol. 20, pp. 103-118, 2010.

[2] A. Ben-Yakar, M. G. Mungal and R. K. Hanson, "Time evolution and mixing characteristics of hydrogen and ethylene transverse jets in supersonic crossfows", *Physics of Fluids*, vol. 18, pp. 026101-1-15, 2006.

[3] M. R. Gruber, A. S. Nejad, T. H. Chen and J. C. Dutton, "Transverse injection from circular and elliptic nozzles into a supersonic crossflow", *J. Propulsion and Power*, vol. 16, issue 3, pp. 449-457, 2000.

[4] V. Viti, R. Neel and J. Schetz, "Detailed flow physics of the supersonic jet interaction flow field", *Physics of Fluids*, vol. 21, pp. 1-16, 2009.

[5] C. F. Chenault and P. S. Beran, "K-ε and Reynolds stress turbulence model comparisons for two-dimensional injection flows", *AIAA J.*, vol. 36, No 8, pp. 1401-1412, 1998.

[6] V. Borovoy, I. Egorov, V. Mosharov, V. Radchenko, A. Skuratov and I. Struminskaya, "Entropy-layer influence on single-fin and double-fin/boundary-layer interactions", *AIAA J.*, vol. 54, No. 2, pp. 443-457, 2016.

[7] V. Ya. Borovoy, I. V. Egorov V. E. Mosharov, V. N. Radchenko, A. S. Skuratov, I. V. Struminskaya, "Shock waves/turbulent boundary layer interference near a fin and a pair of fins at the presence of entropy layer", in *Proc. Int. Conf. Methods of Aerophysical Research, Novosibirsk, Russia,* 2014, pp. 1-9.

[8] M. Ya. Yudelovich. Separation flow. // Encyclopedia of Physics and Technology [Online]. Available: http://femto.com.ua/articles/part_2/2714.html
[9] A. Beketaeva, P. Bruel and A. Naimanova, "Vortical structures behind a transverse jet in a super-sonic flow at high jet to crossflow pressure ratios", *J. Appl. Mech. and Tech. Phys.*, vol. 56, No 5, pp. 777-788–2015.
[10] D. A. Dickmann and F.K. Lu, "Shock/Boundary Layer Interaction Effects on Transverse Jets in Crossflow Over a Flat Plate", in *38th Fluid Dynamics Conference and Exhibit*, Seattle, USA, 2008, Paper AIAA 2008-3723.
[11] R. J. Kee, F. M. Rupley, E. Meeks and J. A. Miller, "CHEMKIN-III: A FORTRAN chemical kinetics package for the analysis of gas-phase chemical and plasma kinetics", SANDIA, Livermore, CA USA, Rep. SAND96-8216, 1996.
[12] K. Karamcheti and M. L. Rasmussen, "Viscous effects far downstream in a slowly expanding hypersonic nozzle", *AIAA J.*, vol. 4, No 5, pp. 807-815, 1966.
[13] T. E. Faber, Fluid Dynamics for Physicists. Cambridge University Press, 2001.
[14] H. Schlichting, *Boundary-layer theory*. McGraw-Hill, 1979.
[15] L. G. Loytsyanskiy, Mechanics of liquids and gases. Pergamon Press, Oxford, 1966.
[16] T. J. Poinsot and S. K. Lele, "Boundary conditions for direct simulation of compressible viscous flows", *J. Comp. Phys.*, vol. 101, pp. 104-129, 1992.
[17] P. Bruel and A. Naimanova, "Computation of the normal injection of a hydrogen jet into a supersonic air flow", *Thermophys. and Aeromech.*, vol. 17, No 4, pp. 531-542, 2010.
[18] Ye. Moisseeva and A. Naimanova, "Supersonic flow of multicomponent gaseous mixture with jet injection", *Comp. Tech.*, vol. 19, No 5, pp. 51-66, 2014.
[19] R. P. Fedkiw, B. Merriman and S. Osher, "High accurate numerical methods for thermally perfect gas flows with chemistry", *J. Comp. Phys.*, vol. 132, pp. 175-190, 1997.
[20] R. C. Rogers, "A study of the mixing of hydrogen injected normal to a supersonic airstream", NASA, Washington, United States, Rep. TN D-6114, 1971.
[21] Z. X. Gao and C. H. Lee, "Numerical research on mixing characteristics of different injection schemes for supersonic transverse jet", *Sci. China. Tech. Sci.*, vol. 54, No 4, pp. 883-893, 2011.
[22] J. R. Henry, E. H. Andrews, Jr., S. Z. Pinckney and C. R. McClinton, "Boundary layer and starting problems on a short axisymmetric scramjet inlet", *Compressible Turbulent Boundary Layers*, pp. 481-508, 1968, NASA SP-216.